The Effect of Halogen Substitution in Self-Assembled Monolayers of 4-Mercaptobiphenyls on Noble Metal Substrates

A. Shaporenko,[†] K. Heister,[†] A. Ulman,[‡,§] M. Grunze,[†] and M. Zharnikov*[,†]

Angewandte Physikalische Chemie, Universität Heidelberg, Im Neuenheimer Feld 253, 69120 Heidelberg, Germany, and Department of Chemical Engineering, Polytechnic University, Brooklyn, New York 11201

Received: October 18, 2004

Self-assembled monolayers (SAMs) formed from 4′-substituted 4-mercaptobiphenyls X-$(C_6H_4)_2$SH (X-BPT, with X = I, Cl, and F) on polycrystalline (111) gold and silver substrates have been characterized by synchrotron-based high-resolution X-ray photoelectron spectroscopy and angle-resolved near-edge X-ray absorption fine structure spectroscopy. The X-BPT molecules were found to form highly oriented and densely packed SAMs on both substrates, with a smaller molecular inclination in the case of Ag. The experimental data show clear evidence for the charge transfer between the 4′-substituent and biphenyl moieties with the direction and extent of the transfer depending on the electronegativity of the halogen substituent. At the same time, no direct evidence of the charge transfer between the 4′-substituent and the thiolate group was observed. However, the substitution of the 4′-hydrogen by a halogen atom seems to affect the detailed packing arrangements of the SAM constituents.

1. Introduction

During last two decades, self-assembled monolayers (SAMs) attracted considerable attention since they allow the preparation of organic surfaces with a specific chemical identity and provide a means to tailor surface properties such as wetting, adhesion, lubrication, corrosion, and biocompatibility.[1−5] In addition, these films can also be used to prepare micro- and nanostructured substrates for sensor applications and fundamental studies on the interaction of proteins and cells with artificial surfaces.[5,6]

So far, most attention was focused on aliphatic SAMs and, above all, on films of *n*-alkanethiols (AT) on noble metal substrates.[3,4] However, recently, aromatic SAMs became of interest (for example, refs 7−22) in view of their applications, including chemical lithography[6,23−25] and molecular electronics.[8,26,27] For many applications, it is highly desirable to form aromatic SAMs with specific substitutions at the 4′-position.[11−14] In particular, a series of SAMs formed from 4′-substituted 4-mercaptobiphenyls with 17 different substitutions has been fabricated on gold and silver substrates and characterized by infrared reflection absorption spectroscopy (IRRAS) and contact angle measurements.[19] Being useful, these techniques have, however, intrinsic limitations and provide often limited and indirect information on the systems under investigation.

In the present work, we performed a detailed spectroscopic characterization of 4′-substituted 4-mercaptobiphenyls X-$(C_6H_4)_2$-SH (X-BPT) with a halogen substitution (X = I, Cl, and F) on polycrystalline (111) gold and silver substrates. We applied two experimental techniques, namely, synchrotron-based high-resolution X-ray photoelectron spectroscopy (HRXPS) and angle-resolved near-edge X-ray absorption fine structure (NEXAFS) spectroscopy. These techniques provide complementary information on the chemical composition and structure of the investigated films.

Our interest in the halogen substitutions was initiated by the hypothesis that the character of the 4′-substituent affects the bonding of the thiol headgroup to the metal substrate and consequently the adsorption kinetics and the equilibrium structure of the aromatic SAMs.[22] This is supposed to originate from the conjugation between the adsorbed thiolate and a 4′-substituent (mediated by the biphenyl backbone), which may affect the electron density on the former species. The use of different halogens at the 4′-position allows us to vary the electronegativity of the substituent to a large extent and, thus, measure the proposed effect.

In the following section, we describe the experimental procedure and techniques. The results are presented and briefly discussed in section 3. An extended analysis of the data is given in section 4 followed by a summary in section 5.

2. Experimental Section

The synthesis of 4′-substituted 4-mercaptobiphenyls is described elsewhere.[19] The gold and silver substrates were prepared by thermal evaporation of 200 nm of gold or 100 nm of silver (99.99% purity) onto mica. These films are standard substrates for thiol-derived SAMs. They are polycrystalline, with a grain size of 20−50 nm as observed by atomic force microscopy. The grains predominantly exhibit a (111) orientation, which is, in particular, supported by the observation of the corresponding forward-scattering maxima in the angular distributions of the Au 4f and Ag 3d photoelectrons[28] and by the characteristic binding energy (BE) shift of the Au 4f surface component.[29] The SAMs were formed by immersion of freshly prepared substrates into a 10 μM X-BPT solution in absolute ethanol at room temperature for 24 h. After immersion, the samples were carefully rinsed with pure ethanol, blown dry with argon, and kept for several days in argon-filled glass containers until

* Author to whom correspondence should be addressed. Phone: +49-6221-544921. Fax: +49-6221-546199. E-mail: Michael.Zharnikov@urz.uni-heidelberg.de.

[†] Universität Heidelberg.

[‡] Polytechnic University.

[§] Current address: Department of Chemistry, Bar-Ilan University, Ramat Gan 52900, Israel

10.1021/jp040667y CCC: $30.25
Published on Web 02/10/2005

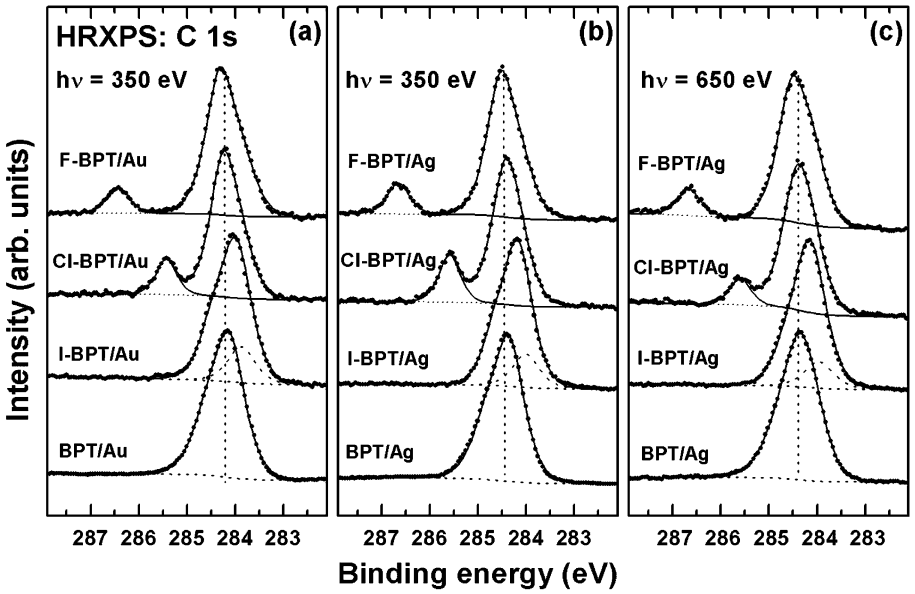

Figure 1. Normalized C 1s HRXPS spectra of F-BPT, Cl-BPT, I-BPT, and BPT on Au (a) and Ag (b,c) acquired at photon energies of 350 eV (a,b) and 650 eV (c). The positions of the main emission for BPT/Au and BPT/Ag are marked by the dotted lines. The emission related to the carbon atom bonded to the halogen substitution is shown in every spectrum.

characterization at the synchrotrons. No evidence for impurities or oxidative degradation products was found.

The fabricated films were characterized by synchrotron-based HRXPS and NEXAFS spectroscopy. All experiments were performed at room temperature. The measurements were carried out under UHV conditions at a base pressure better than 1.5×10^{-9} mbar. The spectra acquisition time was selected in such a way that no noticeable damage by the primary X-rays occurred during the measurements.[6,30−32]

The HRXPS experiments were performed at the bending magnet beamline D1011 at the MAX II storage ring of the MAX-lab synchrotron radiation facility in Lund, Sweden. The HRXPS spectra were acquired in normal emission geometry at photon energies (PE) of 350 and 650 eV for the C 1s range and PEs of 195, 204, and 350 eV for the S 2p region. The F 1s, Cl 2p, and I $3d_{5/2}$ spectra were acquired at PEs of 750, 300, and 680 eV, respectively. The binding energy (BE) scale of every spectrum was individually calibrated using the Au $4f_{7/2}$ emission line of AT-covered Au substrate at 83.95 eV. The latter value is the latest ISO standard.[33] It is very close to a value of 83.93 eV, which has been obtained by us for Au $4f_{7/2}$ using a separate calibration to the Fermi edge of a clean Pt foil.[29] The energy resolution was better than 100 meV, which is noticeably smaller than the full widths at half-maximum (fwhm) of the photoemission peaks addressed in this study. Thus, these fwhms are representative for the natural widths of the respective lines.

HRXPS spectra were fitted by symmetric Voigt functions and either a Shirley-type or linear background. To fit the S $2p_{3/2,1/2}$ and Cl $2p_{3/2,1/2}$ doublets, we used a pair of such peaks with the same fwhm, the branching ratio of 2 ($2p_{3/2}/2p_{1/2}$), and spin−orbit splittings (verified by fit) of ∼1.18 eV and ∼1.8 eV for S 2p and Cl 2p, respectively.[34] The fits were performed self-consistently; the same peak parameters were used for identical spectral regions. The accuracy of the resulting BE/fwhm values is 0.02−0.03 eV.

The NEXAFS measurements were performed at the HE-SGM beamline of the synchrotron storage ring BESSY II in Berlin, Germany. The spectra acquisition was carried out at the C K-edge in the partial electron yield mode with a retarding voltage of −150 V. Linear polarized synchrotron light with a polarization factor of ∼82% was used. The energy resolution was ∼0.40 eV. The incidence angle of the light was varied from 90° (***E*** vector in surface plane) to 20° (***E*** vector near surface normal) in steps of 10°−20° to monitor the orientational order of the X-BPT molecules in the SAMs.

The raw NEXAFS spectra were normalized to the incident photon flux by division through a spectrum of a clean, freshly sputtered gold sample. In the case of Ag substrate, a spectrum of clean silver was subtracted from the raw spectrum of a SAM sample before the normalization.[35,36] The energy scale was referenced to the pronounced π_1* resonance of highly oriented pyrolytic graphite (HOPG) at 285.38 eV.[37]

3. Results

3.1. HRXPS. The HRXPS spectra of F-BPT, Cl-BPT, I-BPT, and nonsubstituted 4-mercaptobiphenyl (BPT, $C_6H_5-C_6H_4-SH$) on Au and Ag are presented in Figures 1−3. These spectra are normalized to allow a better comparison between the different systems. The data for the BPT SAMs are given as a reference. The results of a quantitative analysis of the presented spectra are compiled in Table 1.

In Figure 1, the C 1s HRXPS spectra of X-BPT on Au (a) and Ag (b,c) acquired at photon energies of 350 eV (a,b) and 650 eV (c) are depicted. The spectra of the F-BPT and Cl-BPT SAMs consist of the main emission (marked by the dotted lines for BPT/Au and BPT/Ag) assigned to the biphenyl backbone and an additional peak ascribed to the carbon atom bonded to the 4′-substituent. The BE position of the main emission is somewhat higher for F-BPT as compared to Cl-BPT (see also Table 1), which is related to the higher electronegativity of fluorine as compared to chlorine (Table 2),[38] resulting in the larger charge transfer from the biphenyl moiety in the case of F-BPT. The intensity ratios (I_{add}/I_{main}) between the main and additional peaks are in good agreement with theoretical ratios of 1:6 and 1:8.2 for spectra measured at PEs of 350 and 650 eV, respectively, which confirms the spectra interpretation. Note that the theoretical values were calculated assuming an upright orientation of the biphenyl moieties and using the position parameters for the carbon atoms reported by Brock and Haller.[39] The attenuation lengths of the C 1s photoelectrons in hydro-

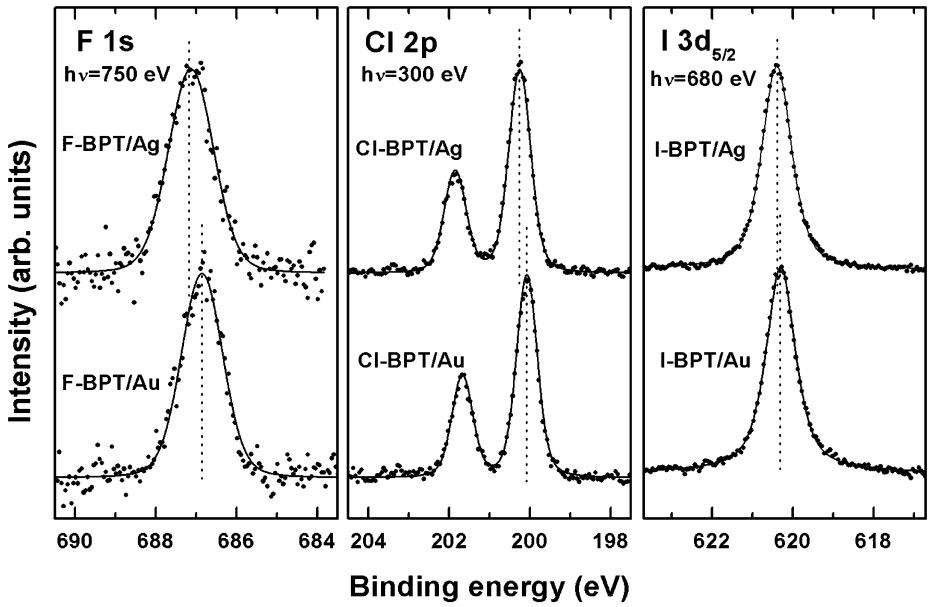

Figure 2. Normalized F 1s, Cl 2p, and I $3d_{5/2}$ HRXPS spectra of F-BPT, Cl-BPT, and I-BPT, respectively, on Au and Ag. The spectra were acquired at different photon energies, slightly (by 60−100 eV) over the respective binding energies. The positions of the emissions are marked by the dotted lines.

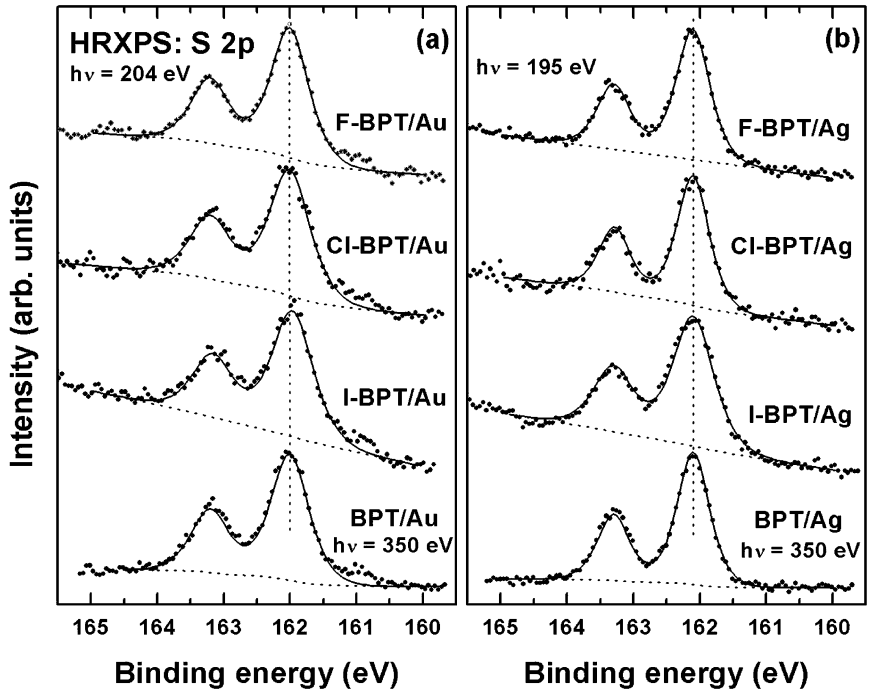

Figure 3. Normalized S 2p HRXPS spectra of F-BPT, Cl-BPT, I-BPT, and BPT on Au (a) and Ag (b) acquired at photon energies of 204 eV (Au), 195 eV (Ag), and 350 eV (BPT). The BE positions of the S 2p doublet (S $2p_{3/2}$) are marked by the dotted lines. A background is shown.

carbon overlayers at PEs of 350 and 650 eV were taken as 6.0 and 13.1 Å, respectively.[40]

The spectra of the I-BPT and BPT films exhibit only the main emission peak (marked by the dotted lines). The BE position of this peak is close to that for the Cl-BPT film in the case of BPT and shifted to a lower BE in the case of I-BPT (see also Table 1). Through use once more of the electronegativity arguments, it is then obvious that these positions are in a better accord with the Allred−Rochow electronegativity scale than with the Pauling electronegativity scale (Table 2).[38] Thus, our results support the former scale.

The emission originating from the 4′-carbon (seen as the additional peak for F-BPT and Cl-BPT) merges with the main emission peak in the case of I-BPT. Assuming a lower electronegativity of iodine as compared to carbon according to the Allred−Rochow scale, one can expect a "hidden" additional peak at the low BE side of the main emission, due to the charge transfer from iodine to the adjacent carbon. This peak is indicated in the spectra of the I-BPT SAMs in Figure 1. The exact BE position of this peak could only be tentatively derived from the photoemission data.

As clearly seen in Figure 1, the main emission peak is somewhat asymmetric, with the degree and character of the asymmetry varying from one film to another. The reason for the asymmetry is a "fine structure" of the main emission (similar to the case of AT SAMs),[41] stemming from different chemical shifts and different screening of the photoemission hole for different carbon atoms along the biphenyl backbone and the

TABLE 1: BE Positions and Fwhm's (in Brackets) of the Photoemission Peaks for X-BPT/Au and X-BPT/Ag

	C 1s main $h\nu = 350$ eV	C 1s add $h\nu = 350$ eV	C 1s I_{main}/I_{add} 350 eV	C 1s I_{main}/I_{add} 650 eV	S $2p_{3/2}$	I $3d_{5/2}$, Cl $2p_{3/2}$, F 1s
BPT/Ag	284.30 (0.84)				162.08 (0.57)	
I-BPT/Ag	284.22 (0.73)	~284.0			162.08 (0.71)	620.35 (0.79)
Cl-BPT/Ag	284.32(0.77)	285.54 (0.51)	4.4	8.7	162.07 (0.57)	200.20 (0.64)
F-BPT/Ag	284.38 (0.84)	286.60 (0.54)	6.9	7.8	162.07 (0.59)	687.08 (1.28)
BPT/Au	284.11 (0.84)				162.02 (0.67)	
I-BPT/Au	284.07 (0.86)	~283.85			161.99 (0.72)	620.25 (0.83)
Cl-BPT/Au	284.12 (0.78)	285.38 (0.50)	6.3		162.00 (0.72)	200.04 (0.61)
F-BPT/Au	284.16 (0.87)	286.38 (0.54)	9		162.00 (0.67)	686.83 (1.13)

TABLE 2: Comparison of the Electronegativity According to the Allred−Rochow and Pauling Scales and the Binding Energy Shift of the C 1s Emission Related to the 4′-Carbon in the X-BPT Films (with Respect to the Main Emission)[a]

substitution	I	Cl	F
Allred−Rochow electronegativity scale	2.21 (−0.29)	2.83 (+0.33)	4.10 (+1.6)
Pauling electronegativity scale	2.66 (+0.11)	3.16 (+0.61)	3.98 (+1.43)
BE shift of the 4′-carbon (X-BPT/Au)	−0.22 eV	+1.26 eV	+2.22 eV
BE shift of the 4′-carbon (X-BPT/Ag)	−0.22 eV	+1.22 eV	+2.22 eV

[a] In brackets, the "relative" electronegativity with respect to carbon (2.50 and 2.55 for the Allred−Rochow and Pauling scales, respectively) is given.

occurrence of shake up excitation in the aromatic matrix.[29,42] The exact analysis of the asymmetry requires, however, an extended parameter variation, including the length of the aromatic chain, and is beyond the scope of the present study.

The C 1s data are complemented by the normalized F 1s, Cl 2p, and I $3d_{5/2}$ HRXPS spectra of F-BPT, Cl-BPT, and I-BPT on Au and Ag, which are presented in Figure 2. These spectra exhibit clear signatures of the 4′-substituents (see Table 1 for the exact parameters). Interestingly, the BE of the I $3d_{5/2}$ emission for both I-BPT/Au (620.25 eV) and I-BPT/Ag (620.35 eV) is higher than the BE of I_2 (619.9 eV),[34] which suggests electron transfer from the iodine atom in agreement with the conclusions derived from the C 1s spectra. Comparing the spectra for the films on Au and Ag, one sees that the F 1s, Cl 2p, and I $3d_{5/2}$ emissions are shifted to lower BE for Au as compared to those for Ag. This shift can be related to different screening of the photoemission hole by the substrate electrons. Considering the observed BE position difference between Au and Ag, one can assume that the 4′-substituent-substrate spacing, which is close to the film thickness, is longer for the films on Ag. Interestingly, the BE positions of the main C 1s emission (Figure 1 and Table 1) exhibit a similar difference between Au and Ag, supporting the "screening" hypothesis. Note that the 350 eV spectra (panels a and b in Figure 1) are mostly characteristic for the upper part of the films due to the small probing depth of the HRXPS at the given kinetic energy of the photoelectrons.

Along with the results on the hydrocarbon matrix and 4′-substituent, information on the SAM-substrate interface is of importance. This information is provided by the S 2p HRXPS spectra of X-BPTs on Au and Ag, which are depicted in Figure 3. All of these spectra exhibit a single S $2p_{3/2,1/2}$ doublet commonly assigned to the thiolate species,[29,43] with no evidence for disulfides, alkylsulfides, or oxidative products; there is, however, a very weak signal from atomic sulfur (161.0 eV for S $2p_{3/2}$)[44] for the films on Au. The BE positions of the "thiolate" doublet (S $2p_{3/2}$) are around 162.00 eV for Au and 162.07 eV for the Ag substrate, almost independent of the 4′-substituent within the accuracy of the experiment. The observed BE difference between Au and Ag is smaller than those for the C 1s, F 1s, Cl 2p, and I $3d_{5/2}$ emissions and is presumably related to the exact electron structure of these metals so that the above hypothesis about the different screening of the C 1s, F 1s, Cl 2p, and I $3d_{5/2}$ photoemission holes is still valid. As to the S 2p spectra, it has been shown recently that the contributions related to the charge transfer upon thiolate−metal bond formation (i.e., initial state effects) and to the hole screening (i.e., final state effects) have comparable effects on the exact BE position of the respective S 2p doublet.[45]

Along with the BE position, an important parameter is the fwhm of the S $2p_{3/2}$ and S $2p_{1/2}$ components. Since the instrumental spreading is negligible in the present case, the value of the fwhm is representative for the natural spreading of the S $2p_{3/2,1/2}$ lines and the inhomogeneity of the bonding configurations or the distribution of the absorption sites for the thiolate headgroups. For a commensurate 2D arrangement with the same absorption site for all thiolate moieties, this value is approximately 0.50 eV (the natural broadening),[42] which is noticeably smaller than the fwhm values presented in Table 1. Thus, the coexistence of several different absorption sites can be assumed for all investigated films on both Au and Ag. Comparing the values for the films formed from the nonsubstituted and 4′-substituted BPTs, one sees a small effect of the substitution in most cases. The fwhm's increase (with respect to BPT) is especially pronounced in the case of iodine so that this substituent provides the largest effect on 2D arrangements of the SAM constituents.

Note that the S $2p_{3/2,1/2}$ fwhm, which we observe for the BPT films is noticeably larger than 0.50 eV, which suggests the coexistence of several different absorption sites in the SAMs formed from the nonsubstituted biphenylthiols. Whereas the formation of a commensurate $\sqrt{3} \times \sqrt{3}$ lattice by the BPT molecules is considered to be possible on Au(111),[29,46] this structure seems to be rather nonreproducible so that we observed several different values of the S $2p_{3/2,1/2}$ fwhm for BPT/Au during last three years.[29] Even variation of the film preparation temperature did not result in a reproducible decrease of the fwhm down to 0.50 eV.

Apart from the above consideration, the intensities of the emission lines have to be addressed. Because of the difficulties with the exact adjustment of the samples and relatively low photon energies used, the accuracy of the intensity values derived from our HRXPS data is somewhat lower as compared to standard laboratory XPS equipment. Therefore, we prefer to report only general trends and do not present the exact intensity and film thickness values for every SAM under the investigation. Generally, for both Au and Ag, we observed approximately the same intensities of both the adsorbate and the substrate

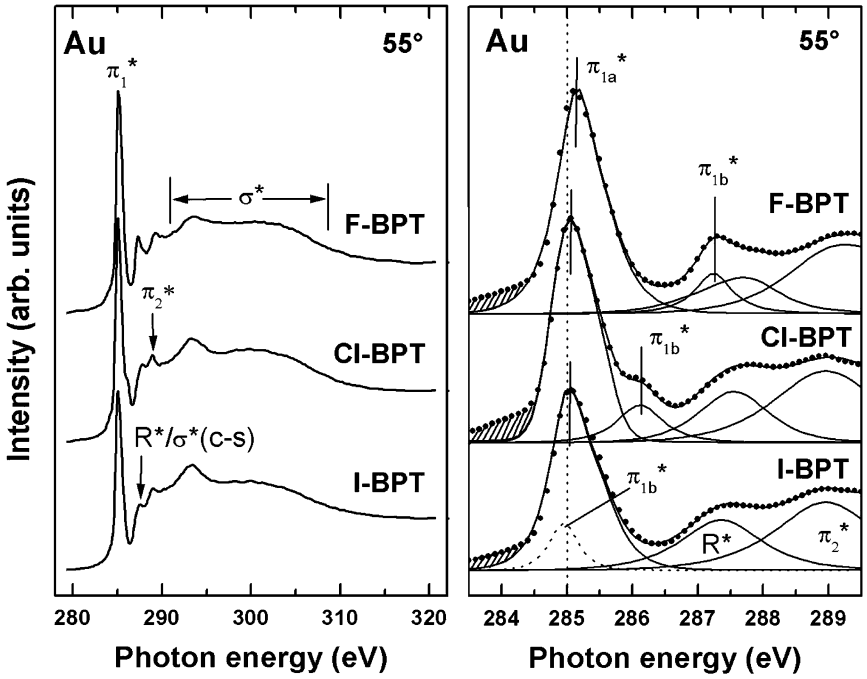

Figure 4. Carbon K-edge NEXAFS spectra of F-BPT, Cl-BPT, and I-BPT on Au over a large energy range (left panel) and close to the absorption edge (right panel). The spectra were acquired at a X-ray incident angle of 55°. The absorption resonances are marked. A decomposition of the spectra into individual contributions is shown in the right panel.

TABLE 3: Assignments and PE Positions of the Characteristic NEXAFS Resonances for X-BPT/Au and X-BPT/Ag

Au and Ag[a]	π_{1a}* ±0.03 eV	π_{1b}* ±0.05 eV	R*/C−S* ±0.1 eV	π_2* ±0.1 eV	σ_1* ±0.2 eV	σ_2* ±1.0 eV	step
BPT[17]	285.00		287.4	288.9	∼293.1	∼300	∼287
I-BPT[c]	285.11	∼285.0	287.33	288.95	∼293.1	∼301	290.1
Cl-BPT[b]	285.13	286.12	287.53	288.97	∼293.3	∼301	290.1
F-BPT[b]	285.20	287.23	287.65	289.15	∼293.4	∼302	290.1

[a] The resonance assignment is performed in accordance with refs 17, 20, 21, and 47−49. There is no noticeable difference in the resonance positions between the films on Au and Ag substrates. [b] Resonance is split in two peaks. [c] The π_{1a}* and π_{1b}* resonances merge.

emissions, independent of the 4′-substituent. However, the intensities of almost all of the SAM-related peaks were slightly higher (by 5−10%) in the case of Ag as compared to those of Au. The film thicknesses derived on the basis of the C 1s, Au 4f, and Ag 3d emissions were within 11.7−13 Å, with slightly larger values in the case of the Ag substrate. For the evaluation, the attenuation lengths reported in ref 40 were used. The derived thicknesses correlate rather well with previous estimates of 12.4 Å for BPT/Au[8] and 13 ± 1 Å for differently substituted X-BPT/Au and X-BPT/Ag.[19]

3.2. NEXAFS. In a NEXAFS experiment, core level electrons (e.g., C 1s for a C K-edge spectrum) are excited into nonoccupied molecular orbitals, which are characteristic for a specific bond, a functional group, or a molecule. The PE positions of the respective absorption resonances give a clear signature of these entities. In addition, information on molecular orientation can be derived from the experimental data, since the cross section of the resonant photoexcitation process depends on the orientation of the electric field vector of the linearly polarized synchrotron light with respect to the molecular orbital of interest (so-called linear dichroism in X-ray absorption).[47] For analysis of the spectral features, it is however useful to exclude the effects of molecular orientation, for which purpose the spectrum acquired at the so-called magic angle of the light incidence (∼55°) is considered. For this particular geometry, the spectrum is independent of the molecular orientation.

Carbon K-edge NEXAFS spectra of I-BPT, Cl-BPT, and F-BPT on Au and Ag acquired at an X-ray incident angle of 55° are presented in Figures 4 and 5, respectively. The spectra are given both over a large energy range (left panels) and close to the absorption edge (right panels). The latter spectra are decomposed into individual absorption resonances, marked in the figure. The parameters of these resonances and higher PE features (σ* resonances; see below) are given in Table 3, in which the data for the BPT SAMs on Au and Ag are also presented as a reference.

The spectra in Figures 4 and 5 are dominated by the intense π_1* resonance of the phenyl rings at ∼285 eV, which is accompanied by the respective π_2* resonance at ∼288.9 eV, the R*/C−S* resonance at ∼287.5 eV, and several broad σ* resonances at higher photon energies (see Table 3 for details). Due to the chemical shifts associated with the halogen substitution, the π_1*, resonance in the Cl-BPT and F-BPT films is split into the π_{1a}* and π_{1b}* resonances, whereas a merger of these two resonances can be assumed in the case of I-BPT so that the π_{1b}* resonance is drawn only tentatively in the latter case. The splitting of the π_1* resonance correlates obviously with the electronegativity of the 4′-substituent, just in the same way as it occurs in the C 1s HRXPS spectra in Figure 1. Also, the lack of an additional resonance in the NEXAFS spectrum of I-BPT fully correlates with the observation of the single emission peak in the respective C 1s HRXPS spectrum. The splitting of the π_{1a}* and π_{1b}* resonances in the Cl-BPT and F-BPT SAMs (∼1.0 and ∼2.05 eV, respectively) agrees very well with the BE spacing between the main and substituent-related emissions in the C 1s HRXPS spectra of these films (∼1.2 and ∼2.2 eV,

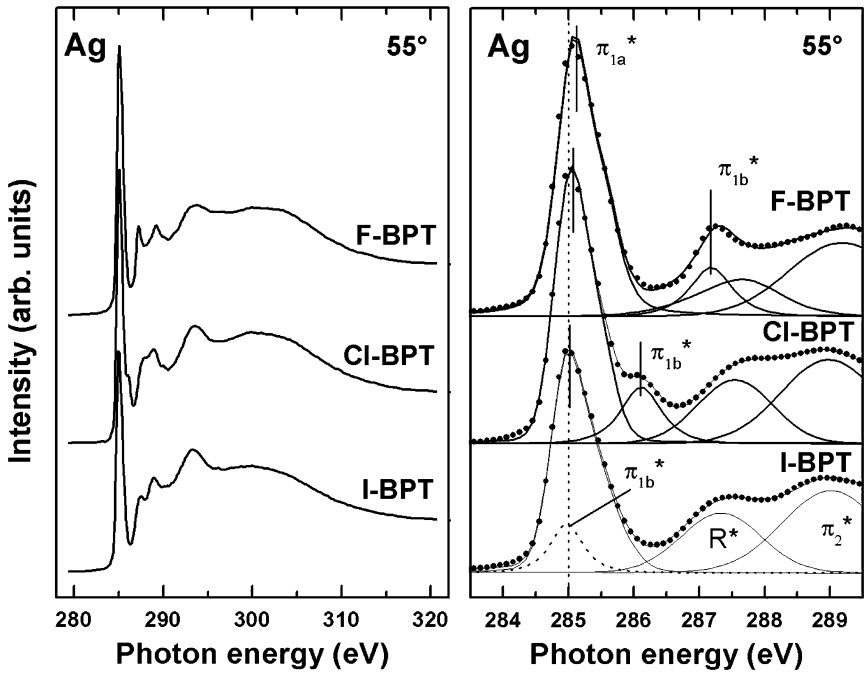

Figure 5. Carbon K-edge NEXAFS spectra of F-BPT, Cl-BPT, and I-BPT on Ag over a large energy range (left panel) and close to the absorption edge (right panel). The spectra were acquired at X-ray incident angles of 55°. The absorption resonances are marked. A decomposition of the spectra into individual contributions is shown in the right panel.

respectively). Note that similar ligand-mediated splitting of the π_1* resonance was also observed for other phenyl-based aromatic molecules such as aniline ($C_6H_5NH_2$),[50] phenol (C_6H_5-OH),[50] and monofluorobenzene (C_6H_5F).[48] In addition, the carbon atoms linked to the first carbon atom coupled to the substituent also experience a perceptible influence of the ligand group. This is evidenced by the increase of the asymmetry and fwhm of the π_{1a}* resonance by going from I-BPT to F-BPT.

The NEXAFS spectra of all X-BPT films exhibit a pronounced linear dichroism, i.e., a dependence of the absorption resonance intensity on the incidence angle of the X-rays, which suggests a high orientational order in these SAMs. Through use of the spectra acquired at different incidence angles (not shown), average tilt angles of the biphenyl backbones in the X-BPT films can be derived. For this purpose, the intensity of absorption resonances I should be monitored as a function of the X-ray incidence angle θ and the resulting dependence evaluated according to theoretical expression (for a vector-type orbital)[47]

$$I(\alpha,\theta) = A\left\{P\frac{1}{3}\left[1+\frac{1}{2}(3\cos^2\theta-1)(3\cos^2\alpha-1)\right]+(1-P)\frac{1}{2}\sin^2\alpha\right\} \quad (1)$$

where A is a constant, P is a polarization factor of the X-rays, and α is the average tilt angle of the molecular orbital.

For the evaluation, the π_1*/π_{1a}* resonance as the most intense one in the spectra has been selected; the transition dipole moment of this resonance is oriented perpendicular to the ring plane. The expression (eq 1) was slightly modified to include the parameters, which determine the orientation of the biphenyl backbones

$$\cos\alpha = \cos\vartheta\sin\varphi \quad (2)$$

where φ is the tilt angle of the molecular axis with respect to the surface normal and ϑ is the twist angle of the aromatic rings with respect to the plane spanned by the surface normal and the molecular axis.[51,52] A herringbone packing of these backbones with a twist angle of 32° close to that for bulk aromatic compounds was assumed.[9,13,53,54] Note that a herringbone structure of the aromatic moieties optimizes the intermolecular interaction in the densely packed 2D layers and is in particular typical for aromatic SAMs on Au.[13,54]

To avoid normalization problems, the intensity ratios $I(\theta)$/$I(20°)$ rather than the absolute intensities were analyzed,[47] where $I(\theta)$ and $I(20°)$ are the intensities of the π_1*/π_{1a}* resonance at X-ray incidence angles of θ and 20°. The angular dependences of the π_1* or π_{1a}* (for F and Cl) resonance intensity ratio $I(\theta)$/$I(20°)$ for the X-BPT films are presented in Figure 6, along with the best theoretical fits according to the eq 1. The derived values of the average tilt angles (φ) of the biphenyl backbones in the X-BPT films are given in Table 4; the accuracy of these values is $\pm 3-5°$, which is just a general accuracy of the NEXAFS experiment and data evaluation. For comparison, the analogous parameters of the BPT SAMs on Au and Ag are presented; the respective tilt angles were derived within the same assumptions as in the present study.[17] As follows from Table 4, the 4′-substituent does not affect the molecular tilt in the X-BPT films to a noticeable extent. The effect of the substrate is, however, clearly visible, since all of the values for the gold substrate are by several degrees higher than the analogous values for the silver one. Taking the derived tilt angles and the molecular lengths, the film thicknesses were evaluated; the results are presented in Table 5. These results correlate rather well with the analogous values calculated on the basis of the HRXPS data (see previous section).

4. Discussion

The HRXPS and NEXAFS data suggest the formation of contamination-free, well-defined, and densely packed X-BPT SAMs on Au and Ag (X = F, Cl, I). The molecules are bound to the substrate via a thiolate linkage, whereas the biphenyl backbones have an upright orientation with an average tilt angle of about 19−22° for Au and 17−19° for Ag.

Both HRXPS and NEXAFS spectra exhibit clear evidence of the charge transfer (electrons) between the halogen atom at

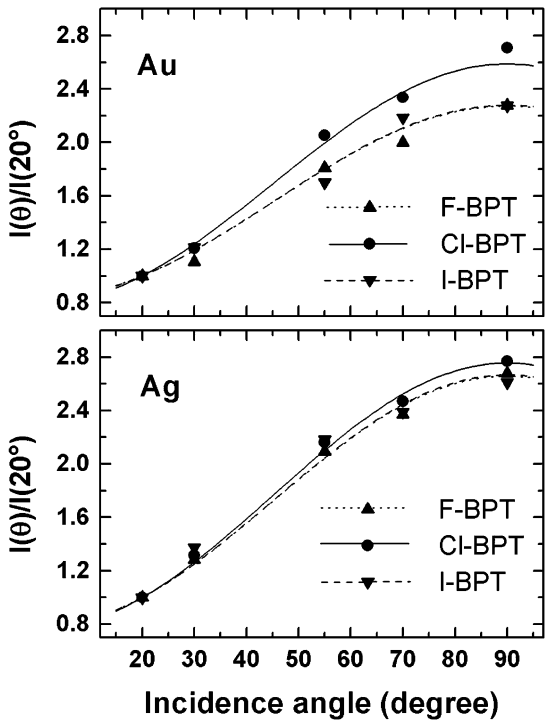

Figure 6. The angular dependence of the π_1* (for I) and π_{1a}* (for F and Cl) resonance intensity ratio $I(\theta)/I(20°)$ for F-BPT (up triangles), Cl-BPT (circles), and I-BPT (down triangles) on Au (upper panel) and Ag (bottom panel) along with the best theoretical fits according to eq 1 (dotted, solid, and dashed lines for F-BPT, Cl-BPT, and I-BPT, respectively).

TABLE 4: Average Molecular Tilt Angle (deg)[a]

	I-BPT	Cl-BPT	F-BPT	BPT[17]
Au	21.8	18.5	21.3	23.0
Ag	19.5	17.3	17.8	18.0

[a] Twist angle 32°, error ±3−5°.

TABLE 5: Effective Film Thicknesses (Å) Calculated on the Basis of the NEXAFS Data Assuming the Lengths of the F-BPT, Cl-BPT, and I-BPT Molecules of 10.45, 10.87, and 11.4 Å[a]

	F-BPT	Cl-BPT	I-BPT	BPT	BPT[17]
Au	11.9	12.6	12.86	11.7	11.8 (XPS)
Ag	12.1	12.7	13.1	12.1	12.1 (XPS)

[a] The S−Au distance is taken as 2.4 Å.[55,56] The values for the BPT SAMs (this work and ref 17) are given for comparison.

the 4′-position and biphenyl moieties. In the HRXPS spectra, these are the additional peaks and the substituent-dependent shift of the main emission. In the NEXAFS spectra, these are the substituent-dependent broadening and splitting of the characteristic π_1* resonance. The position and character of the spectral features indicate that the electron transfer occurs from the rings to the substituent in the case of F and Cl (a larger effect for fluorine) and from the substituent to the rings in the case of iodine. This observation was explained on the basis of the electronegativity of the 4′substituent, which is higher than that of carbon in the case of F (especially high) and Cl and lower than that of carbon in the case of iodine, in accordance with the Allred−Rochow electronegativity scale. The alternative Pauling electronegativity scale disagrees with our data.

No direct evidence for the charge transfer from the 4′-substituent to the thiolate group or from the latter group to the substituent was observed. For both Au and Ag, the binding energy of the thiolate species in the X-BPT films almost does not depend on the identity of the 4′-substituent and is very close to the value for the SAMs formed from the nonsubstituted BPT. At the same time, the HRXPS data imply that the substitution of the 4′-hydrogen by a halogen atom affects the packing arrangements of the SAM constituents, this effect being especially pronounced in the case of iodine. It can not, however, be concluded whether and to what extent does the electronegativity of the 4′-substituent, along with the respective dipole moment, affect the adsorption kinetics of the 4′-substituted biphenyls on noble metal substates. As mentioned in section 1, there is some indirect evidence for such effects.[12,14,22]

The experimental data show a clear substrate effect. The HRXPS spectra of all X-BPT films on Au exhibit a small (but noticeable) downward shift of all emission peaks as compared to Ag. Also, according to the NEXAFS data, the X-BPT molecules are less tilted in the case of Ag. This result correlates with the estimates of the effective thickness performed on the basis of the HRXPS data and with the difference in the screening of the photoemission holes at and close to the SAM−ambient interface in the X-BPT films on Au and Ag. Note that a smaller inclination of the molecular backbones in aromatic thiol-derived SAMs was observed earlier.[17] As mentioned, the respective difference in the molecular tilt between Au and Ag is noticeably smaller in the aromatic SAMs as compared to that of the aliphatic ones, which is mostly related to the difference in the balance of the structural forces in these systems.[21]

5. Conclusion

We performed a detailed characterization of the X-BPT SAMs (X = F, Cl, and I) on polycrystalline (111) gold and silver substrates using HRXPS and NEXAFS spectroscopy. All SAMs were found to be well-defined, densely packed, and contamination-free. The molecules were found to bind to the substrate via a thiolate linkage, whereas the biphenyl backbones have an upright orientation with an average tilt angle of about 19−22° for Au and 17−19° for Ag.

The experimental data show clear evidence for the charge transfer between the 4′-substituent and biphenyl moieties with the direction and extent of the transfer depending on the electronegativity of the halogen substituent in accordance with the Allred−Rochow electronegativity scale. No direct spectroscopic proof of the charge transfer from the 4′-substituent to the thiolate group or from the latter group to the substituent was observed, although there is an indirect evidence that the substitution of the 4′-hydrogen by a halogen atom affects the exact packing arrangements of the SAM constituents.

Except for the difference in molecular tilt, there is a substrate-dependent binding energy shift of all emission peaks in the HRXPS spectra. In addition to these shifts, the emission related to the SAM−ambient interface are additionally shifted, which was ascribed to the larger spacing between the respective photoemission hole and the electron pool of the substrate in the case of Ag.

The obtained results demonstrate the potential of advanced spectroscopic techniques for the characterization of thin organic films and polymer surfaces.

Acknowledgment. We thank Ch. Wöll (Universität Bochum) for providing us with the experimental equipment for the NEXAFS measurements, L. S. O. Johansson (Karlstad University) for the cooperation at MAX-lab, M. Buck and P. Cyganic (St. Andrews University) for the help with the sample preparation, A. Küller (Universität Heidelberg) for providing us with BPT, and the BESSY II and MAX-lab staff for their assistance

during the synchrotron-based experiments. This work has been supported by the German BMBF (GRE1HD and 05KS4VHA/4), European Community (Access to Research Infrastructure action of the Improving Human Potential Program), and the Fonds der Chemischen Industrie.

References and Notes

(1) Ulman, A. *An Introduction to Ultrathin Organic Films: Langmuir−Blodgett to Self-Assembly*; Academic Press: New York, 1991.
(2) Ulman, A. *Chem. Rev.* **1996**, *96*, 1533.
(3) *Thin Films: Self-Assembled Monolayers of Thiols*; Ulman, A., Ed.; Academic Press: San Diego, CA, 1998.
(4) Schreiber, F. *Prog. Surf. Sci.* **2000**, *65*, 151.
(5) Schreiber, F. *J. Phys.: Condens. Matter.* **2004**, *16*, R881.
(6) Zharnikov, M.; Grunze, M. *J. Vac. Sci. Technol., B* **2002**, *20*, 1793.
(7) Sabatani, E.; Cohen-Boulakia, J.; Bruening, M.; Rubinstein, I. *Langmuir* **1993**, *9*, 2974.
(8) Tour, J. M.; Jones, L., II; Pearson, D. L.; Lamba, J. S.; Burgin, T. P.; Whitesides, G. M.; Allara, D. L.; Parikh, A. N.; Atre, S. V. *J. Am. Chem. Soc.* **1995**, *117*, 9529.
(9) Dhirani, A.-A.; Zehner, W.; Hsung, R. P.; Guyot-Sionnest, P.; Sita, L. *J. Am. Chem. Soc.* **1996**, *118*, 3319.
(10) Tao, Y.-T.; Wu, C.-C.; Eu, J.-Y.; Lin, W.-L. *Langmuir* **1997**, *13*, 4018.
(11) Kang, J. F.; Jordan, R.; Ulman, A. *Langmuir* **1998**, *14*, 3983.
(12) Kang, J. F.; Liao, S.; Jordan, R.; Ulman, A. *J. Am. Chem. Soc.* **1998**, *120*, 9662.
(13) Himmel, H.-J.; Terfort, A.; Wöll, Ch. *J. Am. Chem. Soc.* **1998**, *120*, 12069.
(14) Kang, J. F.; Ulman, A.; Liao, S.; Jordan, R. *Langmuir* **1999**, *15*, 2095.
(15) Ishida, T.; Choi, N.; Mizutani, W.; Tokumoto, H.; Kojima, I.; Azehara, H.; Hokari, H.; Akiba, U.; Fujihira, M. *Langmuir* **1999**, *15*, 6799.
(16) Leung, T. Y. B.; Schwartz, P.; Scoles, G.; Schreiber, F.; Ulman, A. *Surf. Sci.* **2000**, *458*, 34.
(17) Frey, S.; Stadler, V.; Heister, K.; Zharnikov, M.; Grunze, M.; Zeysing, B.; Terfort, A. *Langmuir* **2001**, *17*, 2408.
(18) Ishida, T.; Mizutani, W.; Azehara, H.; Sato, F.; Choi, N.; Akiba, U.; Fujihira, M.; Tokumoto, H. *Langmuir* **2001**, *17*, 7459.
(19) Kang, J. F.; Ulman, A.; Liao, S.; Jordan, R.; Yang, G.; Liu, G.-y. *Langmuir* **2001**, *17*, 95.
(20) Fuxen, C.; Azzam, W.; Arnold, R.; Witte, G.; Terfort, A.; Wöll, Ch. *Langmuir* **2001**, *17*, 3689.
(21) Zharnikov, M.; Grunze, M. *J. Phys.: Condens. Matter*. **2001**, *13*, 11333.
(22) Ulman, A. *Acc. Chem. Res.* **2001**, *34*, 855.
(23) Geyer, W.; Stadler, V.; Eck, W.; Zharnikov, M.; Gölzhäuser, A.; Grunze, M. *Appl. Phys. Lett.* **1999**, *75*, 2401.
(24) Eck, W.; Stadler, V.; Geyer, W.; Zharnikov, M.; Gölzhäuser, A.; Grunze, M. *Adv. Mater*. **2000**, *12*, 805.
(25) Gölzhäuser, A.; Eck, W.; Geyer, W.; Stadler, V.; Weimann, T.; Hinze, P.; Grunze, M. *Adv. Mater.* **2001**, *13*, 806.
(26) Bumm, L. A.; Arnold, J. J.; Cygan, M. T.; Dunbar, T. D.; Burgin, T. P.; Jones, L., II; Allara, D. L.; Tour, J. M.; Weiss, P. S. *Science* **1996**, *271*, 1705.
(27) Adams, D. M.; Brus, L.; Chidsey, C. E. D.; Creager, S.; Creutz, C.; Kagan, C. R.; Kamat, P. V.; Lieberman, M.; Lindsay, S.; Marcus, R. A.; Metzger, R. M.; Michel-Beyerle, M. E.; Miller, J. R.; Newton, M. D.; Rolison, D. R.; Sankey, O.; Schanze, K. S.; Yardley, J.; Zhu, X. *J. Phys. Chem. B* **2003**, *107*, 6668.
(28) Köhn, F. Diploma Thesis. Universität Heidelberg, Heidelberg, Germany, 1998.
(29) Heister, K.; Zharnikov, M.; Grunze, M.; Johansson, L. S. O. *J. Phys. Chem. B* **2001**, *105*, 4058.
(30) Wirde, M.; Gelius, U.; Dunbar, T.; Allara, D. L. *Nucl. Instrum. Methods Phys. Res., Sect. B* **1997**, *131*, 245.
(31) Jäger, B.; Schürmann, H.; Müller, H. U.; Himmel, H.-J.; Neumann, M.; Grunze, M.; Wöll, Ch. *Z. Phys. Chem.* **1997**, *202*, 263.
(32) Heister, K.; Zharnikov, M.; Grunze, M.; Johansson, L. S. O.; Ulman, A. *Langmuir* **2001**, *17*, 8.
(33) *Surface Chemical Analysis—X-Ray Photoelectron Spectrometers—Calibration of the Energy Scales*; ISO 15472; International Organization for Standardization: Geneva, Switzerland, 2001.
(34) Moulder, J. F.; Stickle, W. E.; Sobol, P. E.; Bomben, K. D. *Handbook of X-Ray Photoelectron Spectroscopy*; Chastian, J., Ed.; Perkin-Elmer Corp.: Eden Prairie, MN, 1992.
(35) Frey, S.; Heister, K.; Zharnikov, M.; Grunze, M., Tamada, K.; Colorado, R., Jr.; Graupe, M.; Shmakova, O. E.; Lee, T. R. *Isr. J. Chem.* **2000**, *40*, 81.
(36) Zharnikov, M.; Frey, S.; Heister, K.; Grunze, M. *Langmuir* **2000**, *16*, 2697.
(37) Batson, P. E. *Phys. Rev. B* **1993**, *48*, 2608.
(38) Huheey, J. E. *Inorganic Chemistry*; Harper & Row: New York, 1983.
(39) Brock, C. P.; Haller, K. L. *J. Am. Chem. Soc.* **1984**, *88*, 3570.
(40) Lamont, C. L. A.; Wilkes, J. *Langmuir* **1999**, *15*, 2037.
(41) Heister, K.; Johansson, L. S. O.; Grunze, M.; Zharnikov, M. *Surf. Sci.* **2003**, *529*, 36.
(42) Heister, K.; Rong, H.-T.; Buck, M.; Zharnikov, M.; Grunze, M.; Johansson, L. S. O. *J. Phys. Chem. B* **2001**, *105*, 6888.
(43) Laibinis, P. E.; Whitesides, G. M.; Allara, D. L.; Tao, Y.-T.; Parikh, A. N., Nuzzo, R. G. *J. Am. Chem. Soc.* **1991**, *113*, 7152.
(44) Yang, Y.-W.; Fan, L.-J. *Langmuir* **2002**, *18*, 1157.
(45) Shaporenko, A.; Adlkofer, K.; Johansson, L. S. O.; Ulman, A.; Grunze, M.; Tanaka, M.; Zharnikov, M. *J. Phys. Chem. B* **2004**, *108*, 17964.
(46) Leung, T. Y. B.; Schwartz, P.; Scoles, G.; Schreiber, F.; Ulman, A. *Surf. Sci.* **2000**, *458*, 34.
(47) Stöhr, J. *NEXAFS Spectroscopy*; Springer Series in Surface Science 25; Springer-Verlag: Berlin, 1992.
(48) Hitchcock, A. P.; Fischer, P.; Aharon Gedanken; Robin, M. B. *J. Phys. Chem.* **1987**, *91*, 531
(49) Azzam, W.; Wehner, B. I.; Fisher, R. A.; Terfort, A.; Wöll, Ch. *Langmuir* **2002**, *18*, 7766.
(50) Solomon, J. L.; Madix, R. J.; Stöhr, J. *Surf. Sci.* **1991**, *255*, 12.
(51) Zharnikov, M.; Küller, A.; Shaporenko, A.; Schmidt, E.; Eck, W. *Langmuir* **2003**, *19*, 4682.
(52) Shaporenko, A.; Adlkofer, K.; Johansson, L. S. O.; Tanaka, M.; Zharnikov, M. *Langmuir* **2003**, *19*, 4992.
(53) Chang, S.-C.; Chao, I.; Tao, Y.-T. *J. Am. Chem. Soc.* **1994**, *116*, 6792.
(54) Azzam, W.; Cyganik, P.; Witte, G.; Buck, M.; Wöll, Ch. *Langmuir* **2003**, *19*, 8262.
(55) Kondoh, H.; Iwasaki, M.; Shimada, T.; Amemiya, K.; Yokoyama, T.; Ohta, T.; Shimomura, M.; Kono, S. *Phys. Rev. Lett.* **2003**, *90*, 066102−1.
(56) Roper, M. G.; Skegg, M. P.; Fisher, C. J.; Lee, J. J.; Dhanak, V. R.; Woodruff, D. P.; Jones, R. G. *Chem. Phys. Lett.* **2004**, *389*, 87.